NANO LETTERS

Letter

pubs.acs.org/NanoLett

Wearable Textile Battery Rechargeable by Solar Energy

Yong-Hee Lee,[†,⊥] Joo-Seong Kim,[†,⊥] Jonghyeon Noh,[†,⊥] Inhwa Lee,[‡] Hyeong Jun Kim,[‡] Sunghun Choi,[†] Jeongmin Seo,[‡] Seokwoo Jeon,[§,∥] Taek-Soo Kim,*[,‡,∥] Jung-Yong Lee,*[,†,∥] and Jang Wook Choi*[,†,∥]

[†]Graduate School of EEWS, [‡]Department of Mechanical Engineering, [§]Department of Materials Science and Engineering and [∥]KAIST Institute NanoCentury, Korea Advanced Institute of Science and Technology (KAIST), Daejeon 305-701, Republic of Korea

Supporting Information

ABSTRACT: Wearable electronics represent a significant paradigm shift in consumer electronics since they eliminate the necessity for separate carriage of devices. In particular, integration of flexible electronic devices with clothes, glasses, watches, and skin will bring new opportunities beyond what can be imagined by current inflexible counterparts. Although considerable progresses have been seen for wearable electronics, lithium rechargeable batteries, the power sources of the devices, do not keep pace with such progresses due to tenuous mechanical stabilities, causing them to remain as the limiting elements in the entire technology. Herein, we revisit the key components of the battery (current collector, binder, and separator) and replace them with the materials that support robust mechanical endurance of the battery. The final full-cells in the forms of clothes and watchstraps exhibited comparable electrochemical performance to those of conventional metal foil-based cells even under severe folding−unfolding motions simulating actual wearing conditions. Furthermore, the wearable textile battery was integrated with flexible and lightweight solar cells on the battery pouch to enable convenient solar-charging capabilities.

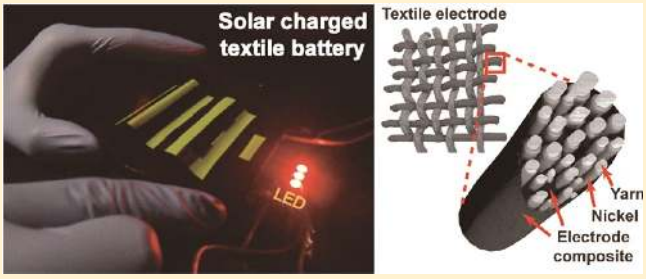

KEYWORDS: *Wearable device, flexible solar cell, lithium ion battery, solar charge*

Smart phones have revolutionized our everyday lives. Smart phones have offered a variety of new functions beyond simple calling abilities, such as gaining access to a variety of information, communicating with others through new concepts of social media, taking photos/videos, listening to music, watching videos, and so forth, influencing every piece of our lives and opening up a new human life pattern. This new life paradigm has driven the development of other future electronic devices, so-called wearable electronics, that fulfill the various functions of smart phones but can be integrated with clothes, eye glasses, wrist watches, and even skin, thus relieving the necessity of separate carriage.[1−3] Hence, wearable electronics certainly represent another paradigm shift in consumer electronics and human life.[4,5]

On the basis of this motivation, diverse electronic devices holding the capability of being flexible, bendable, and stretchable have been demonstrated by engaging new concepts and materials.[6−10] Nevertheless, rechargeable batteries, essential components in powering wearable electronics, have not kept pace with such progress, remaining as a bottleneck in the whole technology.[11,12] The battery community has recognized the lagged situation of the rechargeable batteries and has invested significant efforts. During the course of the research, the community has reached the consensus that for realization of wearable rechargeable batteries, all of the key battery components (electrode, separator, electrolyte) need to be modified to be functional during unusual mechanical motions by finding new materials and harmony between them.[13,14]

In development of wearable rechargeable batteries, the component requiring the most significant alteration from the conventional cell configuration is the current collector because the current collector largely dictates the mechanical properties of the entire cell. Along this direction, one of the most natural approaches would be to use textiles as current collectors after integration with conductive materials. Textile supercapacitors[15] and paper batteries[16] pioneered by the Cui group can be understood in a similar context. Other groups[17−20] have also developed flexible conductive substrates by engaging carbon nanomaterials, such as graphene paper, for demonstration of similar wearable energy storage devices. Although those research findings represent noticeable progress in the given area, the use of carbon nanotubes (CNTs) and graphene imposes a hurdle for real applications; the lowest sheet resistances of the conductive textiles achieved based on the integration of these materials even at maximal percolation are usually higher than ∼10 Ω sq^{-1},[16,21,22] which indicates severe resistances in cell operations and therefore limitations in increasing the cell size and rate performance. Also, CNTs and graphene still have scalability issues although ample attention should help provide rapid progress.[23,24] Because of these limitations of most carbon nanomaterials, metal-incorporating current collectors have also been investigated, and Ag-coated

Received: October 15, 2013
Published: October 28, 2013

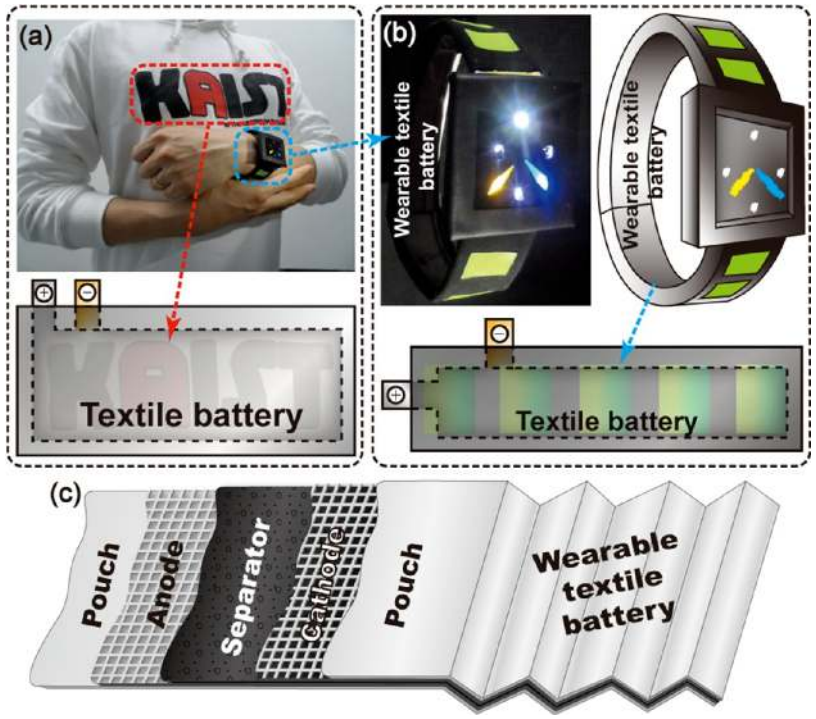

Figure 1. Wearable textile battery. (a) A photograph of wearable textile battery embedded in clothes together with its enlarged view of the inner cell structure. (b) Photograph and schematic representation of a watch with a wearable textile battery strap. (Left) 6 LEDs (1 yellow (= 0.042 W), 1 blue (= 0.062 W), and 4 whites (each = 0.062 W) were lighted up as a demonstration of a functioning watchstrap battery. (c) A schematic illustration of the cell configuration of the wearable textile battery. The key components are based on the materials suitable for flexibility and bendability.

textiles[25,26] and metal wires[27] are most representative. However, not to mention the cost issue of Ag, the Ag-coated textiles have been used only for primary batteries, and metal wires have not been tested under the realistic wearable environments requiring substantial mechanical tolerance perhaps due to fatigue failure. Together with the current collector, both the separator and binder should also be supportive for the active film to endure the aggressive mechanical motions while fulfilling their intrinsic functions.[28] In the present investigation, we have demonstrated a fully functional wearable textile battery by finding unconventional materials for all of the key battery components and integrating them systemically: Ni-coated polyester yarn as a current collector for efficient stress release, polyurethane (PU) binder for strong adhesion of active materials, and PU separator with superior mechanical, electrochemical, and thermal properties. The final full-cell endures extremely severe mechanical tests while delivering comparable electrochemical properties to those of the conventional foil-based counterparts. Furthermore, flexible and lightweight solar cells based on plastic substrates were integrated onto the outer surface of the textile battery for recharging the textile battery without physical connection to power outlet.

Figure 1a illustrates how the present textile battery is integrated with clothes. Utilizing its bendable and foldable capabilities that allow for conformal interfaces with the mother clothes, the textile battery can be either attached onto the clothes or embedded between textile layers. The current textile batteries can also constitute watchstraps (Figure 1b) to serve as power sources of multifunctional future watches that may accompany high energy consumption. To allow the textile batteries to function properly in these unconventional platforms, each cell component adopts new material or structural design (Figure 1c) and will be described in detail from the next paragraph. In addition, the overall fabrication procedure consists of already-existing steps in the conventional cell-assembly and should thus be readily scalable for large-scale manufacturing.

Figure 2a shows a series of photographs of the fabric-based electrode at different stages of the fabrication. Woven polyester yarn was selected as a textile substrate, and Ni was coated onto the surface of each yarn by the established electroless deposition method (EDM). The EDM used in the current study preserves the original morphology of the woven yarn as displayed in Figure 2b. The battery active layers consisting of the active material, binder, and conductive carbon were then coated on the Ni layers. See the Experimental Section for experimental details. As illustrated in Figure 2c, each yarn of the woven textile is made of a bundle of fibers, and the Ni conductive layers and battery active layers are sequentially coated on the surfaces of the fibers. Cross-sectional scanning electron microscopy (SEM) images (Figure 2b inset) confirm conformal coating of Ni layers generated by the EDM. This conformal Ni coating is very critical in battery operations especially with large cell dimensions because the Ni coating determines the electronic conductivity of the textile. The sheet resistance of the Ni-coated textile reaches 0.35 Ω sq^{-1}, which is as small as those of typical metal foils and is also several orders of magnitude smaller than those of conductive paper made of carbon nanomaterials.[21,22] A cross-sectional SEM image and its corresponding elemental mapping (Figure 2d) also verify the conformal and sequential coating of Ni and battery active materials. In addition, cyclic voltammetry (CV) confirms electrochemical stability of the Ni-coated textile in the potential range of 1.0−4.0 V versus Li/Li$^+$ (Supporting Information Figure S1).

dx.doi.org/10.1021/nl403860k | *Nano Lett.* 2013, 13, 5753−5761

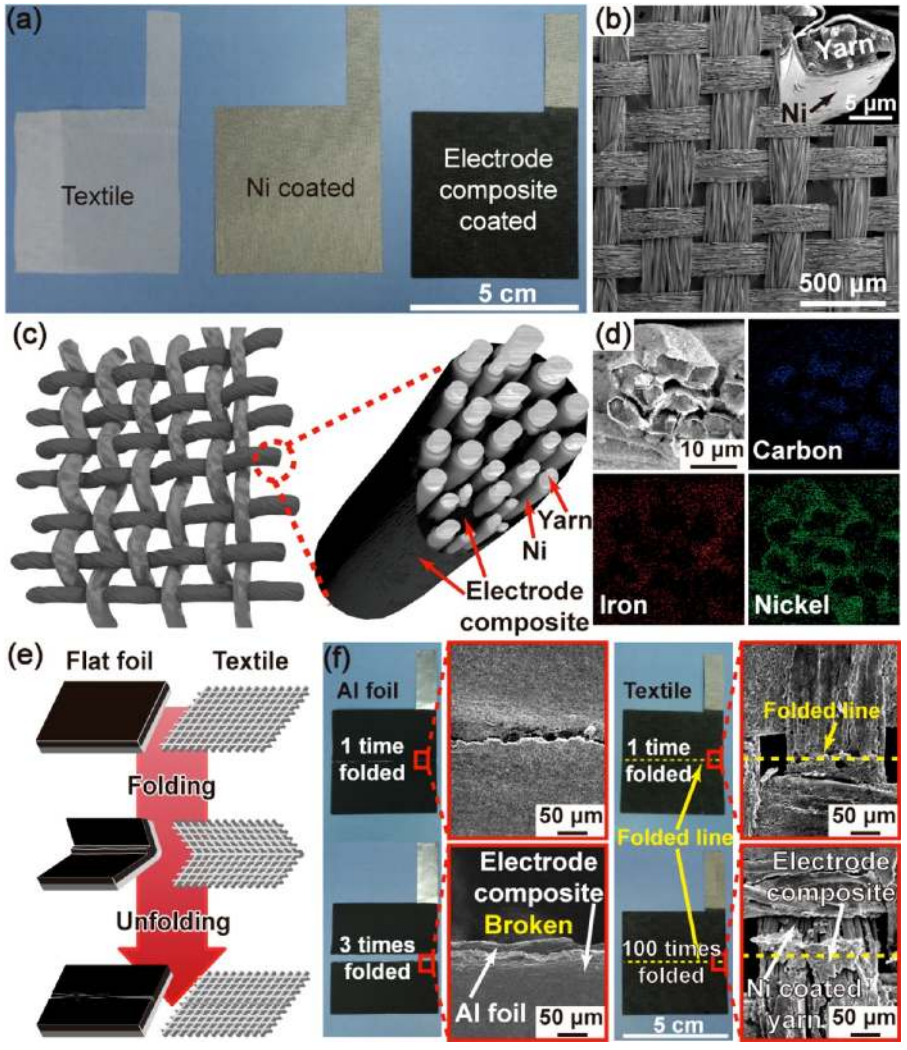

Figure 2. Electrode structure of wearable textile battery and its enhanced folding tolerance. (a) Preparation sequence of the active electrode (5 × 5 cm^2). From left to right: bare polyester yarn substrate, Ni-coated textile substrate by electroless deposition method (EDM), and the final electrode after conformal coating of the electrode composite. (b) The morphology of the Ni-coated textile. (Inset) a cross-sectional SEM images of the same Ni coated textile. (c) A schematic illustration of woven battery electrode yarns. A magnified view indicates that each yarn consisting of multiple strands is coated by Ni and battery composite. (d) A cross-sectional SEM image of the composite electrode textile (top left) together with EDS elemental mapping with regard to carbon, iron, and nickel. (e) A schematic comparison between the electrode based on conventional flat metal foil and the textile battery electrode based on the woven yarn during repeated folding tests. (f) Photographs and SEM images comparatively showing distinctive durability between the foil-based conventional electrode and the textile battery electrode.

Prior to actual battery testing, we assessed the tolerance of each electrode substrate over repeated folding−unfolding (Figure 2e). We chose the repeated folding−unfolding motion as a main mechanics to evaluate the wearable capability of the cell because the folding−unfolding is the most universal movement while wearing clothes and watchstraps. It needs to be emphasized that to simulate extreme situations and thus guarantee robust mechanical sustainability of the cell, the substrate was folded completely until the neighboring units around the folding edge were fully overlapped in each cycle of the folding−unfolding. As shown in Figure 2f, in the case of an Al foil-based battery even after one cycle of folding−unfolding the battery active layer starts to peel off at the folding edge due to the compressional stress toward the edge. The situation becomes worse with repeated cycles, and even after 3 folding−unfolding cycles the Al foil is broken into two pieces along the folding edge. By contrast, the textile battery remains mechanically robust during 100 cycles of the same folding−unfolding utilizing the 3D woven yarn that can release the stress efficiently. The distinctive mechanical stabilities between both cases were also clearly visualized by SEM characterization (Figure 2f).

For the wearable capability of the rechargeable battery, the binder and separator should also support the mechanical endurance of the overall system.[29] In this regard, the binder should assist the electrode film to adhere to the current collector, and the separator is preferred to hold desirable properties in the mechanical stability, electrolyte wettability, and thermal stability. To this end, we decided to investigate unconventional materials rather than modify the existing ones because most of the existing materials have been chosen and developed for conventional flat cells that do not require the wearable capability. After searching a wide range of material candidates, it was found that PU is possessed with various material properties[30,31] suitable for both binder and separator in the wearable battery. Such material properties are originated

dx.doi.org/10.1021/nl403860k | Nano Lett. 2013, 13, 5753−5761

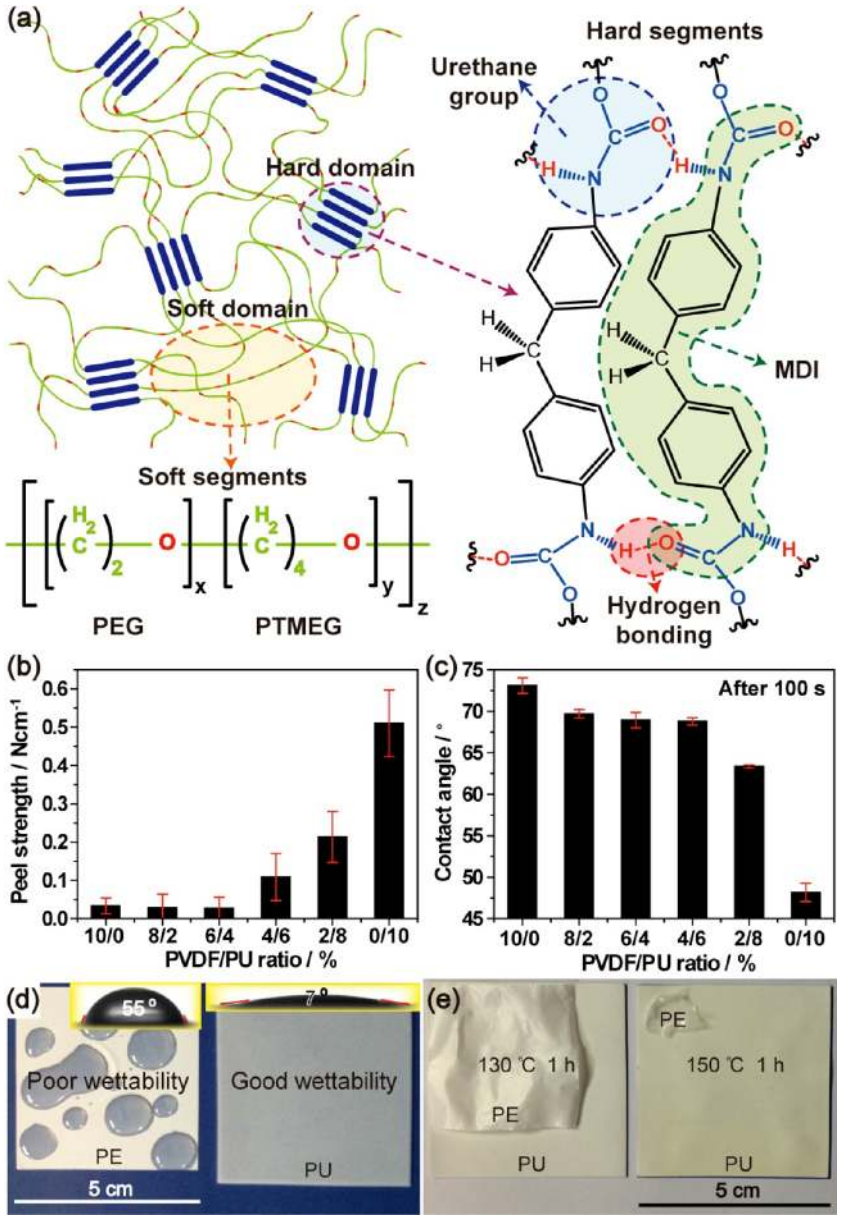

Figure 3. Characterization of polyurethane (PU) binder and separator. (a) A schematic illustration of the PU molecular structure. The PU consists of the hard and soft domains. (b) Peel strength and (c) contact angle tests for the LFP electrode containing various ratios of PU-PVDF binder. The contact angle was measured 100 s after the electrolyte was dropped. (d) Distinctive electrolyte wettability between the PE and PU separators. (Insets) electrolyte contact angles taken 1 s after the electrolyte drop. (e) The thermal shrinkage tests of both separators conducted at different temperatures. The PE separator was overlaid on the PU separator for clear comparison.

from the chemical and polymeric structure of PU in which the hard and soft domains are phase-segregated (Figure 3a). In the hard domains, stiff methylene diphenyl isocyano (MDI) units interact with neighboring ones through hydrogen bonding between the end urethane groups, giving mechanical strength to PU on the whole. By contrast, in the soft domains the soft segments consisting of linearly connected polyethylene glycol (PEG) and polytetramethylene ether glycol (PTMEG) units endow PU with flexible and stretchable capabilities.

In the function of the binder, the hydrogen bonding offered from the urethane groups in the hard segments and dipole−dipole interactions possible with the PEG and PTMEG units of the soft segments support the good adhesion of the electrode films through the enriched interactions between the binder segments as well as between the binder and active materials. The enhanced adhesion was verified by the increased peeling strength as the PU portion increased in the PU/PVDF mixed binder (Figure 3b). The presence of the urethane groups and the PEG/PTMEG units containing oxygen atoms also contributed to good wettability of the both $Li_4Ti_5O_{12}$ (LTO) and $LiFePO_4$ (LFP) electrodes (Figure 3c).

In the function of the separator, while the hard domains support the mechanical strength, the soft domains provide the flexibility (Supporting Information Figure S2a). Hence, a combination of both properties allows for exceptional mechanical strength of the PU separator even during folding and stretching conditions, which is very desirable for its use in the wearable battery. At the same time, similarly to the binder, the urethane groups in the hard domains and the PEG/PTMEG units in the soft domains facilitate efficient Li ion

dx.doi.org/10.1021/nl403860k | *Nano Lett.* 2013, 13, 5753−5761

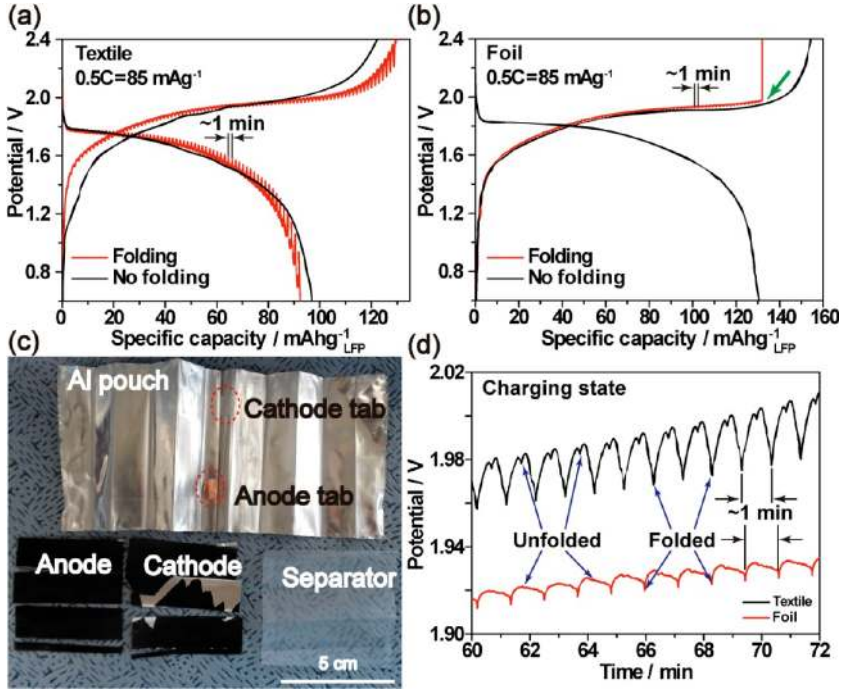

Figure 4. Electrochemical characterization of wearable textile battery. First charge–discharge curves of (a) wearable textile battery and (b) conventional foil-based battery cycled between 0.6 and 2.4 V in LFP-LTO full-cell configuration at a constant current of 85 mA g^{-1}. The red and black lines were attained under with and without folding motion. In (b), the green arrow indicates the point where the foil-based cell stops functioning due to rupture of the substrates. (c) The cell components of the conventional foil-based battery after 1 cycle consisting of 78 folding–unfolding repetitions. (d) Magnified charging profiles of both types of the cells. Each period corresponds to one cycle of folding–unfolding.

diffusion through intimate interaction with the polar electrolyte solvents, which was reflected in various analyses including wettability (Figure 3d), contact angle (Figure 3d insets and Supporting Information Movie S1–S2), electrolyte uptake (Supporting Information Figure S2b), and ionic conductivity (Supporting Information Figure S2c). Notably, the PU separator prepared in the present study showed almost no porosity as indicated by its Gurley time that was out of the measurement range. On the contrary, the PE separator used as a control showed a Gurley time of 200–280 s. The Gurley time herein is defined as the time required for 100 cm^3 of air to pass through the membrane under an air pressure of 0.862 kgf cm^{-2} (Gurley type Densometer, TOYOSEIKI). Such reduced porosity should play a critical role in preventing short-circuits between both electrodes during severe mechanical motions, which could be a serious and nontrivial issue for highly porous conventional separators. Consequently, the decent ionic conductivity of the PU separator even with such negligible porosity is quite exceptional and, once again, originates from its aforementioned microscopic structure. In addition, the PU separator exhibited superior resistance against thermal shrinkage at high temperatures (Figure 3e), which is directly related to the safety of the battery. The remarkably improved thermal stability is also ascribed to the microscopic structure of the PU separator composed of the hard domains responsible for the mechanical strength as well as the hydrogen bonding interactions that result in high melting temperature of PU around 230 °C.

In order to test electrochemical performance of the wearable textile battery consisting of the LTO anode and the LFP cathode under severe mechanical motions, a home-built folding instrument (Supporting Information Figure S3) was used for in situ battery measurements during repeated folding–unfolding. To simulate the severe folding situation, the pouch cell with size of 10 × 11.5 cm^2 was folded every 1.5 cm, and the bending radius (R_c) of each folding unit goes down to 0.65 mm upon complete compression of the instrument (Supporting Information Movie S3). See the Supporting Information Figure S4 for the definition of R_c. Also, each cycle of the complete folding–unfolding takes approximately 1 min. More detailed information about cell fabrication and electrochemical testing is described in the Experimental Section. Figure 4a,b show, respectively, the first charge–discharge curves of the wearable textile battery and the conventional foil-based battery in the presence (and absence) of the folding–unfolding motions. The galvanostatic curve during the folding–unfolding follows almost the same track as that under no motion, indicating overall electrochemical reaction remains preserved during the severe mechanical motions. However, in the case of the foil-based battery, the cell stops the operation in the middle of the first charge, more accurately after 78 cycles of the folding–unfolding (green arrow in Figure 4b), consistent with the folding test in Figure 2f that indicates that the electrode alone without other cell components can be ripped only after several folding–unfolding cycles. When this cell was disassembled after the operation, both electrodes were found to be ripped off along the multiple folding edges (Figure 4c), giving an explanation for the ceased cell operation. Also, the repeated folding–unfolding was reflected by periodic fluctuations of the voltage in the galvanostatic profiles (Figure 4d). Each period of the fluctuation in both types of batteries matches well with the interval of folding–unfolding cycles (~1 min). The observed voltage fluctuations are associated with the distance change between the anode and cathode during the folding–unfolding motion. At the fully compressed position, the distance between both electrodes is the smallest, resulting in the lowest

dx.doi.org/10.1021/nl403860k | Nano Lett. 2013, 13, 5753–5761

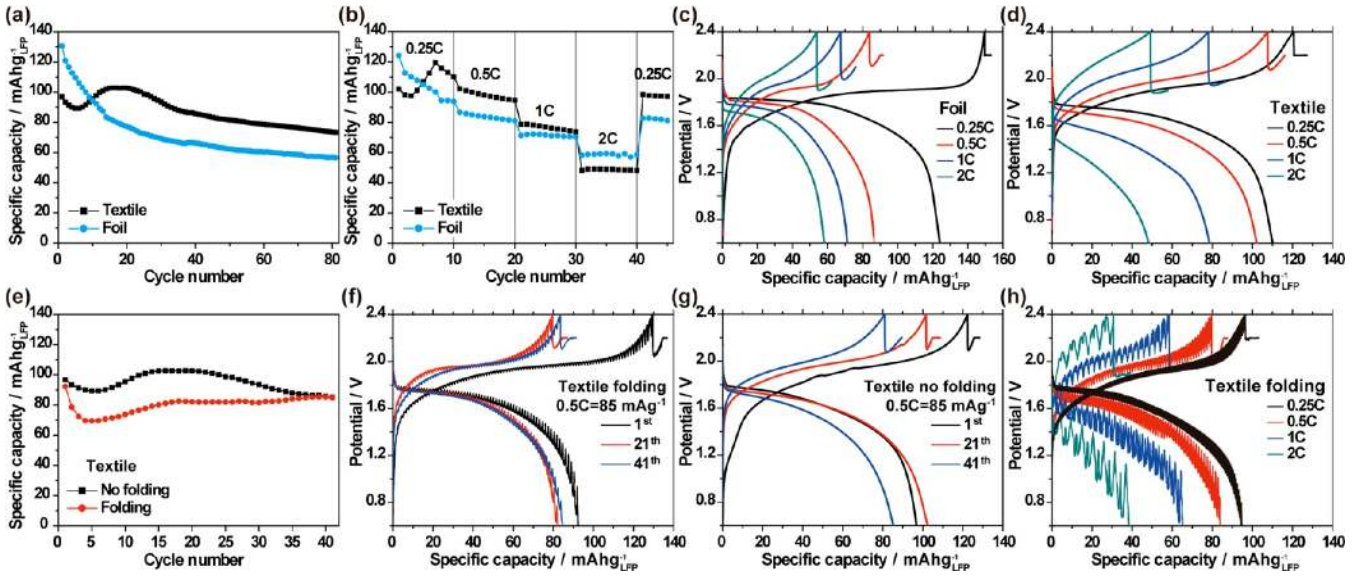

Figure 5. Rate and cycling tests of the wearable textile battery. (a) Cycling and (b) rate performance of the wearable textile battery (black) and the conventional foil-based battery (blue) without any folding–unfolding motions. For the cycling tests, a constant current of 85 mA g^{-1} (= 0.5C) was applied for charge and discharge in each cycle. For the rate performance tests, the C-rate was the same for charge and discharge in each cycle, and the constant current mode was applied. The corresponding voltage profiles of (c) the foil-based battery and (d) the textile battery at different C-rates. (e) The cycling performance of the textile battery with (red) and without (black) repeated folding–unfolding motions. The corresponding potential profiles of the textile battery at different cycle numbers (f) with and (g) without the repeated folding–unfolding motions. (h) The voltage profiles of the textile battery at various C-rates during repeated folding–unfolding motions. The potential range used in all of the data in this figure was 0.6–2.4 V under LFP-LTO full-cell configuration.

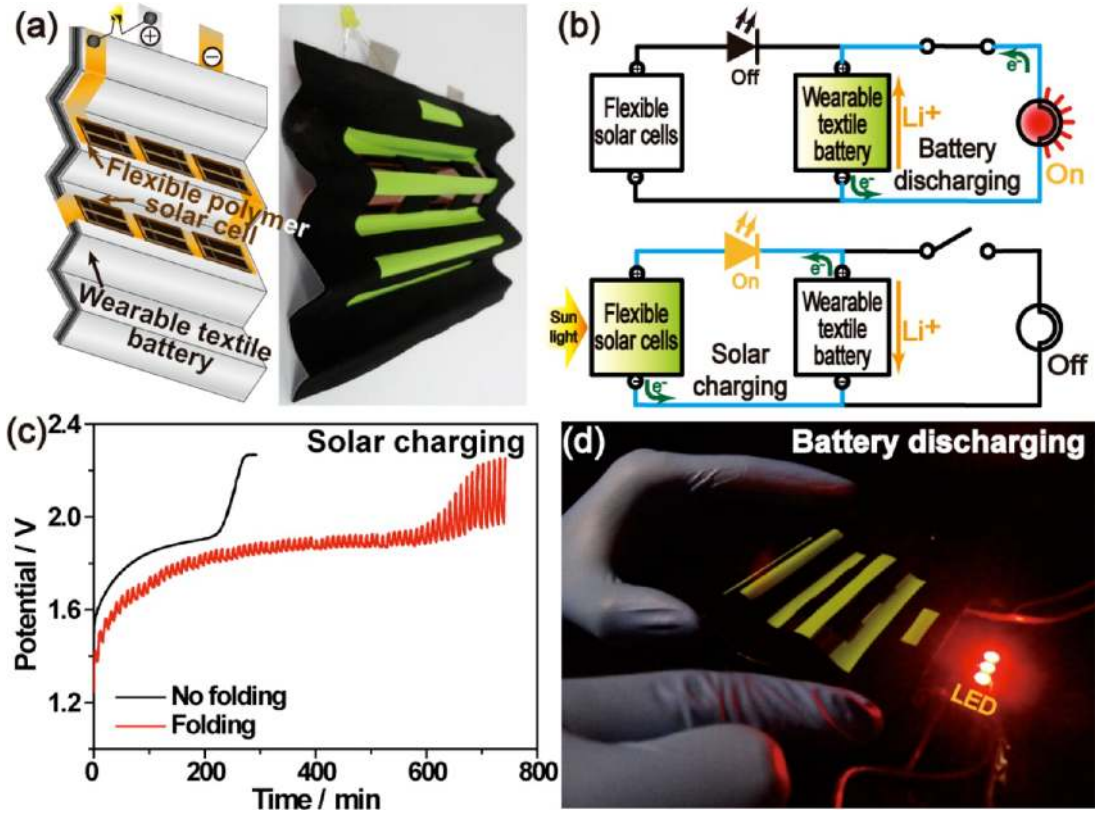

Figure 6. Integration with flexible polymer solar cells. (a) Schematic representation and photograph of the textile battery integrated with polymer solar cells. (b) Equivalent circuits of a solar rechargeable textile battery in the discharging and solar-charging modes. In the discharging mode, the battery turns on light bulbs, and, in the solar-charging mode, the battery is charged, which is indicated by an LED (marked in yellow). (c) Potential profiles of the textile battery during solar-charging in the presence and absence of the repeated folding–unfolding motions. Each folding–unfolding cycle takes 10 min. (d) A demonstration of battery operation. The solar-charged textile battery is capable of lighting up 9 LED bulbs (each LED = 0.042 W).

dx.doi.org/10.1021/nl403860k | *Nano Lett.* 2013, 13, 5753–5761

overpotential during the charging process in Figure 4d. Also, the relatively larger amplitudes of the fluctuations in the textile battery are related to the separator thickness: the PU separator is thicker than the PE separator (180 μm vs 20 μm) and, as a result, the distance change between the anode and cathode is more significant for the PU separator, leading to larger amplitudes of the fluctuations in the galvanostatic curve.

The wearable textile battery also exhibited decent cycling and rate performance (Figure 5). First, without folding−unfolding motions the textile battery showed comparable performance to that of the foil-based counterpart, as summarized in Figure 5 panel a (cycle) and panel b (rate). The comparable performances between both types of batteries were further confirmed by the analogous voltage profiles at various C-rates (Figure 5c,d). More importantly, the wearable textile battery showed good cycling performance even during severe folding−unfolding repetitions. After 40 cycles equivalent to 5500 deep folding−unfolding cycles, the textile battery retained 91.8% of the original capacity, which is similar to the value (88.0%) of the same textile battery but without any mechanical motions (Figure 5e). The relatively lower capacities during the folding−unfolding motions are attributed to the fact that such mechanical motions make ionic transport less efficient at various points of Li diffusion including through the separator, at the electrode−electrolyte interface, and within the electrode films. However, it is still remarkable that the capacity was retained well during the very harsh mechanical conditions. Although several papers have demonstrated flexible Li-ion rechargeable batteries in a full-cell configuration,[13,14,27] most of those works were tested under moderate bending/folding conditions. Moreover, unlike in our investigation electrochemical performances were not monitored simultaneously while mechanical motions were engaged. As in the capacity retention, similar potential profiles (Figure 5f,g) were observed for both experimental conditions throughout cycling, although the voltage fluctuations showed up along the curves when the folding−unfolding motions were engaged. In addition, the textile battery also showed similar rate performances under both conditions with and without the folding−unfolding motions (compare Figure 5d,h), although the specific capacities became a little smaller at all C-rates during the folding−unfolding mode perhaps due to the aforementioned less efficient Li ion diffusion. One noticeable phenomenon is that under the folding−unfolding mode the amplitude of the voltage fluctuation increases at higher C-rates, resulting in increased overpotentials at the higher C-rates, which are associated with fluctuations in the ionic conductivities during each folding−unfolding cycle due to the thickness changes of the PU separator.

For more convenient use of the wearable textile battery, the ability to recharge the battery without the need to disassemble it from the mother clothes is highly desirable. For this, we integrated a series of flexible polymer solar cells with the wearable textile battery, thus circumventing the inconvenience of wiring the battery to a power outlet each time of recharge. As displayed in Figure 6a, series connected solar cells were attached on the battery pouch. Other than the light-accepting area, the device was covered by fabric for cosmetic purposes. The polymer solar cells employ poly[*N*-9-hepta-decanyl-2,7-carbazolealt-5,5-(4,7-di-2-thienyl-2,1,3-benzothiadiazole)] (PCDTBT) and [6,6]-phenyl C71-butyric acid methyl ester ($PC_{70}BM$) as active donor and acceptor materials, respectively. The power conversion efficiency (PCE) of the solar cells (~0.5 cm^2) on polyethylene naphthalate (PEN) substrates was 5.49%, comparable to that on a glass substrate. Its current density−voltage ($J-V$) characteristic and real image are presented in Supporting Information Figure S5.

For stable recharging capabilities, the solar-charging system is required to have a wide range of operating voltage up to 2.4 V while it can supply a stable current level of ~5 mA. As shown in Supporting Information Figure S5a, our solar cells show a current density of ~10 mA cm^{-2} at a voltage of 0.4 V under simulated AM 1.5G illumination at 100 mW cm^{-2}. Hence, we designed the solar recharging system consisting of six series-connected solar cells with the cell area of ~0.5 cm^2. Equivalent circuits in charging and discharging modes and detailed device configuration of the integrated system are presented in Figure 6b and Supporting Information Figure S6, respectively. To ensure decent solar cell operations during unusual mechanical motions, the performance of the solar cells was first examined under the aforementioned light illumination while the integrated system was being folded/unfolded repeatedly (Supporting Information Movie S4). Detailed measurement setup is presented in Supporting Information Figure S7a. As shown in Figure 6c, during the folding−unfolding cycles at a fixed charging rate of 0.3C, the potential profile of the textile battery was elongated compared to that without such folding−unfolding motion. The extended charging period is ascribed to the decreased light absorption of the solar cells during the folding cycles, and it was analyzed quantitatively with respect to the angle of the incident light (Supporting Information Figure S7). In addition, the marked voltage fluctuations (Figure 6c) reflect the fluctuations in the light absorption of the solar cells during the folding−unfolding motion as well as the distance changes between both electrodes, as discussed in Figure 4d. Finally, Figure 6d demonstrates that the fully solar-charged textile battery lights up nine light-emitting diodes (LEDs, power consumption of each LED = 0.042 W) to show a decent operation of the current integrated system.

Apparently, the mechanical endurance of the cell is directly affected by the electrode film thickness, indicating a trade-off relation between folding tolerance and total capacity in mAh. With the given mass loadings of the active materials and cell dimensions, the current wearable textile battery delivers a capacity of ~13 mAh. This value can be, however, increased further by engaging different textiles in which the weaving structures of the yarn (Supporting Information Figure S8) allow for increased mass loadings of active materials without impairing the mechanical stability of the electrode film. As a simple demonstration of such an opportunity, we increased the mass loading by 6 times by using the same textile but by switching the weaving method from plain weave to knit weave[32] and reached a total capacity of 85 mAh with the same cell dimensions while the mechanical tolerance was preserved (Supporting Information Figure S9). These capacities are expected to cover various applications such as watch-type devices, haptic devices, and so forth.[33] But the integration of flexible solar cells with the wearable battery would relieve the capacity requirement substantially because the operation hours of the given devices are not largely restricted by the total capacity during the solar cell operation in daytime.

The present investigation demonstrates that the materials and fabrication processes can be systemically united to realize a wearable textile battery with exceptional mechanical stability particularly in the forms of clothes and watchstraps. It is also expected that further tuning of the cell dimensions will find

dx.doi.org/10.1021/nl403860k | *Nano Lett.* 2013, 13, 5753−5761

various future applications beyond what can be conceptualized now, especially with the aid of solar-charging capabilities.

Experimental Section. *Electroless Nickel Deposition.* The nickel-coated polyester textiles were prepared following the reported procedure.[34] Briefly, polyester fabric was first dipped in 37% HCl containing 26 mM $SnCl_2$ for 10 min at 25 °C. The sample was then immersed in 1.7 mM $PdCl_2$, 37% HCl, and 0.32 M H_3BO_3 at pH 2 for activation. Next, the fabric sample was dipped into an aqueous solution of 97 mM $NiSO_4$, 27 mM trisodium citrate dihydrate, 0.34 M NH_4Cl, and 0.14 M $NaH_2PO_2{\cdot}H_2O$ for electroless nickel deposition. Finally, the nickel-plated fabric was washed with DI water and dried at 150 °C for 20 min. All reagents were purchased from Sigma-Aldrich.

Synthesis of Polyurethane and Its Application for Binder and Separator. Polyurethane (PU) was synthesized based on the following procedure: 0.12 mM 4,4-diphenylmethane diisocyanate (MDI), polytetramethylene glycol (PTMEG), and polyethylene glycol (PEG) at a molar ratio of 4:1:1 were dissolved in dimethylformamide (DMF), and then stirred at 80 °C for 5 h to generate a prepolymer emulsion. Next, 0.06 mM 1,4-butanediol was added to the prepolymer emulsion, and this emulsion was stirred again at 80 °C for 5 h to for further polymerization into the final polymer forms. For use of PU for binder, the final polymer emulsion was completely dried in a vacuum oven at 80 °C for 24 h, and the dried powder was added into the battery slurries. For preparation of the PU separators, the polymer emulsion was cast onto release-paper substrates and was then partially dried. The dried PU films were dipped into water for 2 h to replace DMF with water, and the preparation of the PU separators were completed by removing the release-paper substrates.

Characterization. The morphologies of the textile were characterized using SEM (HITACHI, S-4800), and elemental mapping was done by EDS apparatus attached to the SEM. The sheet resistance of the Ni-coated textile with 10 × 10 cm^2 was measured using a 4-point probe system (FPP-2400, DASOL ENG). For the peeling tests, the specimens were prepared in the size of 10 × 30 mm^2, which were then attached to 3M tape. By pulling the tape at a constant displacement rate of 100 μm s^{-1} (DTS Company), peel strength was continuously monitored. Current density−voltage (J−V) characteristics of the polymer solar cells were measured using a solar simulator (PEC-L12, Peccell Technologies) under 100 mW cm^{-2} from a 150 W Xe short arc lamp filtered by an AM 1.5G filter.

Cell Preparation. For preparation of the active electrodes, the active materials, denka black, and PU binder were dissolved in *N*-methyl-2-pyrrolidone (NMP) in a weight ratio of 80:10:10 (cathode) and 74.4:15.6:10 (anode). Commercial LFP (Hydro-Québec) and LTO (Sigma-Aldrich) were used for the cathode and anode, respectively. The well-mixed slurries were cast onto Ni-coated polyester textiles using the doctor blade technique. The mass loadings of the active materials were 90 and 128 mg for the cathode and anode, respectively, for active areas of 5 × 5 cm^2. The n/p ratio, defined as the actual anode capacity/the cathode capacity, was adjusted to 1.23 for the LTO/LFP full-cells. The electrochemical properties were characterized by preparing aluminum pouch full-cells (pouch size = 10 × 11.5 cm^2). In these cells, PU separators (thickness = 180 μm) and 1 M $LiPF_6$ dissolved in a mixture of ethylene carbonate (EC) and dimethyl carbonate (DMC) (EC/DMC = 1:1 = v/v, Soulbrain) were used as separators and electrolyte, respectively. The final thicknesses of the wearable textile and foil-based batteries were 650 and 360 μm, respectively. The watchstrap battery was prepared based on the same procedures but in smaller dimensions of 1 × 5 cm^2. Two of these watchstrap batteries were connected in series to light up white and blue LEDs (Figure 1b). The conventional foil-based pouch full-cells were prepared by the same procedure, but metal foils, PE separators (Toray Tonen), and PVDF were used as current collectors, separators, and binders, respectively. The cell assembly processes were done in an argon-filled glovebox.

Electrochemical Measurements. The electrochemical properties of all of the batteries were galvanostatically tested in the full-cell potential range of 0.6−2.4 V using a battery cycler (MACCOR series 4000). For the rate performance test, the current density for each period was same for charge and discharge. In all of the pouch full-cell measurements, the charge processes were under CCCV mode such that when the cutoff voltage (2.4 V) was reached, the bias was on hold at 2.2 V for 30 min with a bottom current limit at 0.1C. The electrochemical folding−unfolding tests were measured by using a home-built linear stage machine (QS48, TPC motion). In order to measure ionic conductivities of separators, electrochemical impedance spectroscopy measurements were conducted (Bio-Logic VSP) in the frequency range of 10 mHz to 1 MHz by preparing 2032 coin-type cells. The LSV experiments were conducted in the potential range of 3.0−5.5 V vs Li/Li^+ at a scan rate of 0.05 mV s^{-1} at 25 °C. The C-rates in all of the electrochemical measurements are defined based on 1C = 170 mA g^{-1}.

Preparation and Integration of Solar Cells. Polymer solar cells were fabricated on indium tin oxide (ITO)-coated polyethylene naphthalate (PEN) substrates.[35] Poly(3,4-ethylenedioxythiophene)/poly(styrenesulfonate) (PEDOT/PSS, Al4083, Clevios) layer was spun onto the substrates at 3000 rpm for 30 s, and then the substrates were annealed at 140 °C for 10 min. The PCDTBT/$PC_{70}BM$ (1-materials: nano-c) at a weight ratio of 1:4 in a 1,2-dicholobenzene solution was spun at 1100 rpm for 1 min on the PEDOT/PSS layer, and the samples were dried at 70 °C for 15 min. Subsequently, TiO_x solution was spun at 3000 rpm for 30 s, and they were annealed at 80 °C for 10 min in air. Lastly, 100 nm of Al was deposited through a shadow mask by thermal evaporation on the devices. The active device area was approximately 0.5 cm^2. The solar cells were integrated in series through copper tapes. The binding between the solar cell and copper tape was reinforced by a silver paste (ELCOAT, CANS) and a Kapton double-sided adhesive tape.

■ ASSOCIATED CONTENT

Ⓢ Supporting Information

Further analyses of textile battery, textiles, separators, and polymer solar cells in addition to details of bending radius and solar charging/folding tests. This material is available free of charge via the Internet at http://pubs.acs.org.

■ AUTHOR INFORMATION

Corresponding Authors

*E-mail: (T.-S.K.) tskim1@kaist.ac.kr.
*E-mail: (J.-Y.L.) jungyong.lee@kaist.ac.kr.
*E-mail: (J.W.C.) jangwookchoi@kaist.ac.kr.

Author Contributions

⊥These authors contributed equally to this work.

Notes

The authors declare no competing financial interest.

■ ACKNOWLEDGMENTS

This work was financially supported by the National Research Foundation of Korea (NRF) grant funded by the Korea government (MEST) (NRF-2012-R1A2A1A01011970, NRF-2012- R1A1A1006072, and NRF-2011-0014131). This work was also partially supported by the Technology Innovation Program funded by the Ministry of Trade, industry & Energy (MI, Korea) (MI-2013-10044519).

■ REFERENCES

(1) Chen, Y.; Au, J.; Kazlas, P.; Ritenour, A.; Gates, H.; McCreary, M. *Nature* **2003**, *423* (6936), 136−136.
(2) Lu, X.; Xia, Y. *Nat. Nanotechnol.* **2006**, *1* (3), 163−164.
(3) Kim, D.-H.; Lu, N.; Ma, R.; Kim, Y.-S.; Kim, R.-H.; Wang, S.; Wu, J.; Won, S. M.; Tao, H.; Islam, A. *Science* **2011**, *333* (6044), 838−843.
(4) Hu, X.; Krull, P.; de Graff, B.; Dowling, K.; Rogers, J. A.; Arora, W. J. *Adv. Mater.* **2011**, *23* (26), 2933−2936.
(5) Jung, H. Y.; Karimi, M. B.; Hahm, M. G.; Ajayan, P. M.; Jung, Y. J. *Sci. Rep.* **2012**, 2.
(6) Sun, Y.; Choi, W. M.; Jiang, H.; Huang, Y. Y.; Rogers, J. A. *Nat. Nanotechnol.* **2006**, *1* (3), 201−207.
(7) Kim, D. H.; Kim, Y. S.; Wu, J.; Liu, Z.; Song, J.; Kim, H. S.; Huang, Y. Y.; Hwang, K. C.; Rogers, J. A. *Adv. Mater.* **2009**, *21* (36), 3703−3707.
(8) Kaltenbrunner, M.; White, M. S.; Głowacki, E. D.; Sekitani, T.; Someya, T.; Sariciftci, N. S.; Bauer, S. *Nat. Commun.* **2012**, *3*, 770.
(9) Lee, C. H.; Kim, D. R.; Zheng, X. *Proc. Natl. Acad. Sci. U.S.A.* **2010**, *107* (22), 9950−9955.
(10) Weisse, J. M.; Lee, C. H.; Kim, D. R.; Zheng, X. *Nano Lett.* **2012**, *12* (6), 3339−3343.
(11) Nishide, H.; Oyaizu, K. *Science* **2008**, *4*, 10.
(12) Xu, S.; Zhang, Y.; Cho, J.; Lee, J.; Huang, X.; Jia, L.; Fan, J. A.; Su, Y.; Su, J.; Zhang, H. *Nat. Commun.* **2013**, *4*, 1543.
(13) Kwon, Y. H.; Woo, S. W.; Jung, H. R.; Yu, H. K.; Kim, K.; Oh, B. H.; Ahn, S.; Lee, S. Y.; Song, S. W.; Cho, J. *Adv. Mater.* **2012**, *24* (38), 5192−5197.
(14) Li, N.; Chen, Z.; Ren, W.; Li, F.; Cheng, H.-M. *Proc. Natl. Acad. Sci. U.S.A.* **2012**, *109* (43), 17360−17365.
(15) Hu, L.; Pasta, M.; Mantia, F. L.; Cui, L.; Jeong, S.; Deshazer, H. D.; Choi, J. W.; Han, S. M.; Cui, Y. *Nano Lett.* **2010**, *10* (2), 708−714.
(16) Hu, L.; Choi, J. W.; Yang, Y.; Jeong, S.; La Mantia, F.; Cui, L.-F.; Cui, Y. *Proc. Natl. Acad. Sci. U.S.A.* **2009**, *106* (51), 21490−21494.
(17) Pushparaj, V. L.; Shaijumon, M. M.; Kumar, A.; Murugesan, S.; Ci, L.; Vajtai, R.; Linhardt, R. J.; Nalamasu, O.; Ajayan, P. M. *Proc. Natl. Acad. Sci. U.S.A.* **2007**, *104* (34), 13574−13577.
(18) Gwon, H.; Kim, H.-S.; Lee, K. U.; Seo, D.-H.; Park, Y. C.; Lee, Y.-S.; Ahn, B. T.; Kang, K. *Energy Environ. Sci.* **2011**, *4* (4), 1277−1283.
(19) Wang, K.; Zhao, P.; Zhou, X.; Wu, H.; Wei, Z. *J. Mater. Chem.* **2011**, *21* (41), 16373−16378.
(20) Weng, Z.; Su, Y.; Wang, D. W.; Li, F.; Du, J.; Cheng, H. M. *Adv. Energy Mater.* **2011**, *1* (5), 917−922.
(21) Kaempgen, M.; Chan, C. K.; Ma, J.; Cui, Y.; Gruner, G. *Nano Lett.* **2009**, *9* (5), 1872−1876.
(22) Zheng, G.; Hu, L.; Wu, H.; Xie, X.; Cui, Y. *Energy Environ. Sci.* **2011**, *4* (9), 3368−3373.
(23) Su, M.; Zheng, B.; Liu, J. *Chem. Phys. Lett.* **2000**, *322* (5), 321−326.
(24) Vijayaraghavan, A.; Blatt, S.; Weissenberger, D.; Oron-Carl, M.; Hennrich, F.; Gerthsen, D.; Hahn, H.; Krupke, R. *Nano Lett.* **2007**, *7* (6), 1556−1560.
(25) Gaikwad, A. M.; Zamarayeva, A. M.; Rousseau, J.; Chu, H.; Derin, I.; Steingart, D. A. *Adv. Mater.* **2012**, *24* (37), 5071−5076.
(26) Gaikwad, A. M.; Whiting, G. L.; Steingart, D. A.; Arias, A. C. *Adv. Mater.* **2011**, *23* (29), 3251−3255.
(27) Liu, Y.; Gorgutsa, S.; Santato, C.; Skorobogatiy, M. *J. Electrochem. Soc.* **2012**, *159* (4), A349−A356.
(28) Kil, E. H.; Choi, K. H.; Ha, H. J.; Xu, S.; Rogers, J. A.; Kim, M. R.; Lee, Y. G.; Kim, K. M.; Cho, K. Y.; Lee, S. Y. *Adv. Mater.* **2012**, *25* (10), 1395−1400.
(29) Choi, K.-H.; Kim, S.-H.; Ha, H.-J.; Kil, E.-H.; Lee, C. K.; Lee, S. B.; Shim, J. K.; Lee, S.-Y. *J. Mater. Chem. A* **2013**, *1* (17), 5224−5231.
(30) Kim, Y.; Zhu, J.; Yeom, B.; Di Prima, M.; Su, X.; Kim, J.-G.; Yoo, S. J.; Uher, C.; Kotov, N. A. *Nature* **2013**, *500*, 59−63.
(31) Ghosh, B.; Urban, M. W. *Science* **2009**, *323* (5920), 1458−1460.
(32) Tan, P.; Tong, L.; Steven, G. *Composites Part A* **1997**, *28* (11), 903−922.
(33) Kamijoh, N.; Inoue, T.; Olsen, C. M.; Raghunath, M.; Narayanaswami, C. *Proc. IEEE 5th Int Conf on Wearable Computers* **2001**, 133−140.
(34) Jiang, S.; Kan, C.; Yuen, C.; Wong, W. *J. Appl. Polym. Sci.* **2008**, *108* (4), 2630−2637.
(35) Baek, S.-W.; Noh, J.; Lee, C.-H.; Kim, B.; Seo, M.-K.; Lee, J.-Y. *Sci. Rep.* **2013**, 3.